VERTICAL OSCILLATIONS OF A SOLAR CORONAL LOOP IN A GRAVITATIONALLY STRATIFIED SOLAR CORONA: COMPARISON OF 3D AND 2D CASES

P. Konkol, K. Murawski,

Group of Astrophysics and Gravity Theory, Institute of Physics
UMCS — Maria Curie-Skłodowska University
Radziszewskiego 10, 20-031 Lublin, Poland

(Received March 1, 2010; revised version received May 19, 2010)

We compare impulsively generated vertical oscillations in three-dimensional (3D) and two-dimensional (2D) solar coronal arcade loops. 3D and 2D magnetohydrodynamic equations are solved numerically in the limit of ideal plasma. Numerically obtained wave signatures are analyzed to reveal characteristic spatial and temporal scales. The numerical results show that in 2D case wave period is slightly longer than in 3D one. These results are reminiscent of the recent Hinode data.

PACS numbers: 95.30.Qd, 96.60.Hv, 96.60.P–

1. Introduction

Coronal loops are dense magnetic structures that reside in the solar corona. *Because of strong magnetic forces compared to the hydrostatic pressure mater is trapped along the the field lines creating characteristic smooth bands.* These structures are able to sustain various types of oscillations some of which are interpreted as magnetohydrodynamic (MHD) waves [1]. Among these waves standing fast magnetoacoustic kink oscillations were detected in horizontal [2, 3] and vertical polarizations [4].

Recently, these standing fast magnetoacoustic oscillations became a subject of intensive theoretical investigations. For instance, Verwichte *et al.* [5] considered the loop as a 2D curved magnetic slab and showed that the kink oscillations can be a subject to lateral wave leakage. Andries *et al.* [6] showed numerically that the frequency and spatial structure of the trapped modes were affected by density variations along the loop. Then Andries and also Diáz [6,7] addressed this problem analytically. Gruszecki [8] included a dense photosphere-like layer and found that energy leakage into this layer results in stronger wave attenuation than in the case line-tying boundary conditions, action of this layer is mimicked by implementation [9]. In another approach, Gruszecki, Murawski [10] showed that in the 2D curved coronal loop the effect of gravity results in a decrease of a wave period and in an increase of attenuation time. Ofman [11] discussed horizontal oscillations of an active region loop that was embedded in an isothermal plasma. He found that these oscillations were rapidly attenuated. Pascoe [12] considered, by numerical simulations, impulsively generated horizontal oscillations of a 3D loop. They showed that the fundamental mode of these oscillations exhibited a 30% smaller wave period than the theoretically predicted value [13].

Vertical oscillations of a 3D loop in a gravitationally stratified solar corona have not been studied so far. A main goal of this paper is to perform such studies here and compare the 3D and 2D cases. As analytical treatment does not seem to be amenable we refer to numerical simulations.

This paper is organized as follows. The numerical model is described in Sec. 2. The numerical results are presented and discussed in Sec. 3. This paper is concluded by a presentation of the main results in Sec. 4.

2. Numerical model

Our coronal system is taken to be modeled by the ideal MHD equations:

$$\frac{\partial \varrho}{\partial t} + \nabla \cdot (\varrho \boldsymbol{V}) = 0\,, \tag{1}$$

$$\varrho \frac{\partial \boldsymbol{V}}{\partial t} + (\varrho \boldsymbol{V} \cdot \nabla)\, \boldsymbol{V} = -\nabla p + \varrho \boldsymbol{g} + \frac{1}{\mu}(\nabla \times \boldsymbol{B}) \times \boldsymbol{B}\,, \tag{2}$$

$$\frac{\partial p}{\partial t} + \left(\vec{V} \cdot \nabla\right) p = -\gamma p \nabla \cdot \vec{V}\,, \tag{3}$$

$$\frac{\partial \boldsymbol{B}}{\partial t} = \nabla \times (\boldsymbol{V} \times \boldsymbol{B})\,, \tag{4}$$

$$\nabla \cdot \boldsymbol{B} = 0\,, \tag{5}$$

$$p = \frac{k_{\mathrm{B}}}{m}\, \varrho T\,. \tag{6}$$

Here $\gamma = 5/3$ is the adiabatic index, μ is the magnetic permeability, ϱ is mass density, $\boldsymbol{V}$ is flow velocity, p is gas pressure, $\boldsymbol{g} = (0, 0, g)$ is gravitational acceleration of its value $g = 274\ \mathrm{m\,s^{-2}}$, $\boldsymbol{B}$ is magnetic field, T is temperature, m is mean particle mass, and k_{B} is Boltzmann's constant.

2.1. Equilibrium state

In both 2D and 3D cases we assume that at the equilibrium state the coronal plasma is still ($\boldsymbol{V} = 0$). Then from Eq. (2) we get that

$$-\nabla p_{\mathrm{e}} + \varrho_{\mathrm{e}} \boldsymbol{g} + \frac{1}{\mu}(\nabla \times \boldsymbol{B}_{\mathrm{e}}) \times \boldsymbol{B}_{\mathrm{e}} = 0\,.$$

We assume now that the pressure gradient force is balanced by the gravity. As a result, the Lorentz force has to disappear and the equilibrium is described by the following equations:

$$-\frac{\partial p_{\rm e}}{\partial z} = \varrho_{\rm e} g\,, \tag{7}$$

$$\frac{1}{\mu}(\nabla \times \boldsymbol{B}_{\rm e}) \times \boldsymbol{B}_{\rm e} = 0\,, \tag{8}$$

$$\nabla \cdot \boldsymbol{B}_{\rm e} = 0\,. \tag{9}$$

With a use of the equation of state, Eq. (6), and hydrostatic pressure balance (7) we find:

$$p_{\rm e}(z) = p_0 \exp\left(-\int\limits_{z_{\rm r}}^{z} \frac{dz'}{\tilde{\Lambda}(z')}\right)\,, \qquad \varrho_{\rm e}(z) = \frac{p_{\rm e}(z)}{g\tilde{\Lambda}(z)}\,. \tag{10}$$

Here

$$\tilde{\Lambda}(z) = \frac{k_{\rm B}T(z)}{mg}$$

is the pressure scale-height, and p_0 denotes the gas pressure at the reference level, $z = z_{\rm r} = 10$ Mm. It is noteworthy that gas pressure $p_{\rm e}(z)$ and mass density $\varrho_{\rm e}(z)$ profiles are determined by a temperature profile $T_{\rm e}(z)$ which in our case is adopted as (see *e.g.*, [14])

$$T(z) = \frac{1}{2}T_{\rm c}\left[1 + \frac{T_{\rm ch}}{T_{\rm c}} + \left(1 + \frac{T_{\rm ch}}{T_{\rm c}}\right)\,\tanh\left(\frac{z - z_{\rm t}}{z_{\rm w}}\right)\right]\,. \tag{11}$$

Here $T_{\rm ch} = 10^4$ K denotes chromospheric temperature and $T_{\rm c} = 10^6$ K is temperature of the solar corona that is separated from the chromosphere at the level $z = z_{\rm t} = 4\,{\rm Mm}$ by a transition region of its width $z_{\rm w} = 0.2\,{\rm Mm}$. Despite of its simplicity the above temperature profile is sufficient to adequately describe the solar corona and the chromospheric top layer at the transition region. As a result, a coronal loop can be modeled appropriately.

We assume that equilibrium magnetic field of Eq. (8) is satisfied by current-free ($1/\mu\nabla \times \boldsymbol{B}_{\rm e} = 0$) and potential ($\boldsymbol{B}_{\rm e} = \nabla \times (A\,\hat{\boldsymbol{y}})$) coronal arcade such as [15]

$$[B_{\rm x}, B_{\rm y}, B_{\rm z}] = B_0\left[\cos\left(\frac{x}{\Lambda_{\rm B}}\right), 0, \sin\left(\frac{x}{\Lambda_{\rm B}}\right)\right]\,\exp\left(\frac{-z}{\Lambda_{\rm B}}\right)\,. \tag{12}$$

Here A is a magnetic flux function

$$A(x,y,z) = B_0\Lambda_{\rm B}\cos\left(\frac{x}{\Lambda_{\rm B}}\right)\exp\left(\frac{-z}{\Lambda_{\rm B}}\right)\,,$$

B_0 is the magnetic field at, $z = z_r$, $\Lambda_B = 2L/\pi$ is the magnetic scale-height, and $L = 50$ Mm is the horizontal half-width of the arcade. We define the plasma β as the ratio of gas to magnetic pressures,

$$\beta = \frac{p_0}{B_0^2/2\mu_0} = \frac{\gamma}{2}\left(\frac{c_{sc}}{c_{Ac}}\right)^2,$$

where c_{sc} and c_{Ac} denote respectively sound and Alfvén speeds in the solar corona. We choose and hold fixed $c_{sc} = 100$ km s^{-1} and $c_{Ac} = 10^3$ km s^{-1}. These values give $\beta = 0.012$ at the reference level. At higher altitudes β grows reaching a value of 0.0277 at the loop apex. Fig. 1 shows altitude profile of β. Other equilibrium parameters are listed out in Table I.

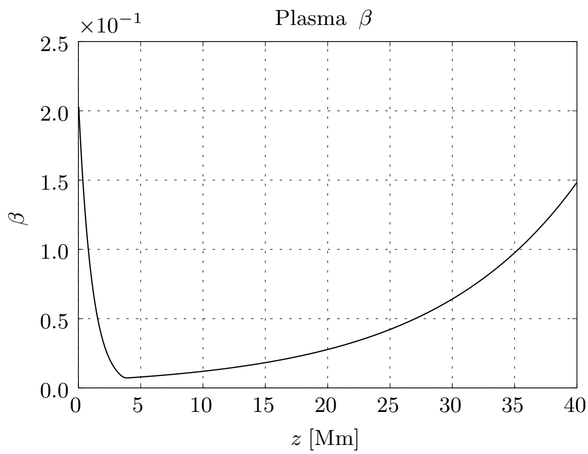

Fig. 1. Plasma β profile.

TABLE I

Equilibrium parameters.

Parameter	Value	Description
g	$274\,\mathrm{m\,s^{-2}}$	gravitational acceleration
z_r	$10\,\mathrm{Mm}$	reference level
c_{Ac}	1×10^6 m s^{-1}	Alfvén speed in the corona
c_{sc}	1×10^5 m s^{-1}	sound speed in the corona
L	$50\,\mathrm{Mm}$	a half-width of the arcade
T_{rat}	1×10^{-2}	temperature ratio, T_{ch}/T_c
z_w	2×10^{-1} Mm	width of the transition region
z_t	$4\,\mathrm{Mm}$	altitude of the transition region

2.2. A coronal loop

We consider a loop that is embedded in the coronal arcade of Eq. (12). A mass density profile of this loop in the 3D case is expressed as

$$\varrho_{\rm l}(x,y,z) \;=\; \varrho_{\rm e} + \tfrac{1}{2}\,\varrho_{\rm e}\,(d-1)\;h(x,z)\,\exp\left(\frac{-(y-y_{01})^2}{2S_{\rm y}^2}\right), \qquad (13)$$

and in the 2D case:

$$\varrho_{\rm l}(x,z) \;=\; \varrho_{\rm e} + \tfrac{1}{2}\,\varrho_{\rm e}\,(d-1)\;h(x,z)\,, \qquad (14)$$

where

$$h(x,z) = \left|\mathrm{erf}\left(\frac{A-A_1}{S_{\rm A}}\right) - \mathrm{erf}\left(\frac{A-A_2}{S_{\rm A}}\right)\right|.$$

This profile of $h(x,z)$ means that in the x–z plane the loop is placed between two magnetic field lines corresponding to two values of magnetic flux functions A_1 and A_2. Those values determine loop's inner and outer edges, respectively and parameter $S_{\rm A}$ determines how narrow or sharp is the border of the loop. Along the y-direction the profile of the loop is defined by the Gauss function with parameter $A_{\rm y}$. The left foot of the loop is located at $y = y_{01} = 7.5$ Mm.

The mass density is enhanced in the loop comparing to the ambient medium. We choose the mass density contrast $d = \varrho_{\rm i}/\varrho_{\rm e} = 10$, where $\varrho_{\rm i}$ denotes the mass density within the loop and $\varrho_{\rm e}$ corresponds to the ambient

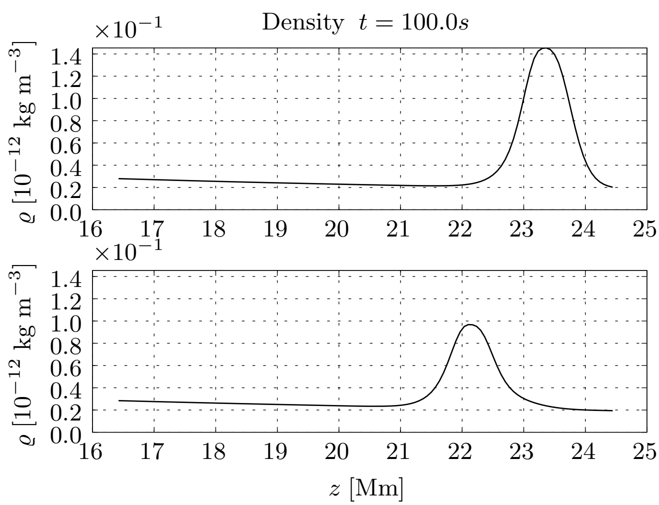

Fig. 2. Mass density profiles at $t = 100$ s for the 2D (top panel) and 3D (bottom panel) cases.

medium. Such a loop does not correspond to any exact equilibrium and for a strongly magnetized plasma, such as the solar corona, it slowly decays in time. The effect is more significant in the 3D case Fig. 2.

Both in the 2D and 3D cases the loops do not have a perfect circular shape (Fig. 3), but their average radius and length can be estimated as 20 Mm and 63 Mm, respectively. These values are close to the observationally determined data of Ofman, Wang [16].

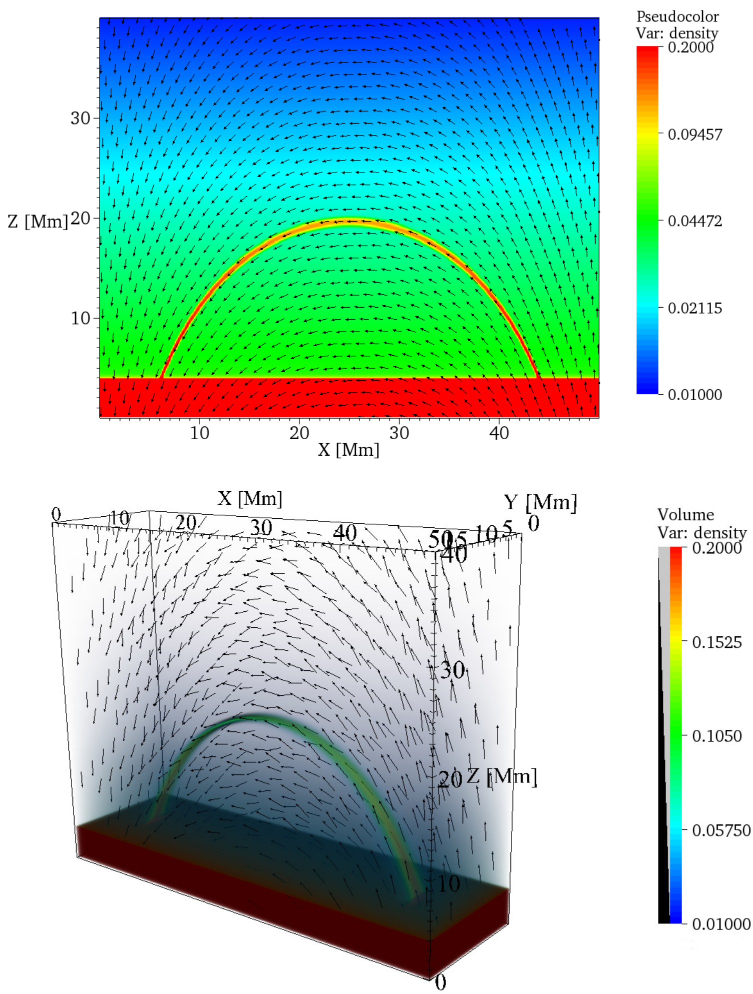

Fig. 3. A general structure of 2D (top panel) and 3D (bottom panel) loops. The density unit is $[10^{-12}\,\mathrm{kg\ m^{-3}}]$.

2.3. Impulsive perturbations

To trigger vertical loop oscillations we launch initially at $t = 0$, the Gaussian pulse in a velocity component $\delta\mathrm{V}_\perp$ that is perpendicular to $\boldsymbol{B}$. In both 2D and 3D cases we choose

$$\delta\mathrm{V}_\perp(x, y, z, t = 0) \;=\; A_\mathrm{m}\; f(x, y, z)\; \frac{\boldsymbol{B}}{B_\phi}\,, \tag{15}$$

where

$$f(x, y, z) = \exp\left[-\left(\frac{x - x_0}{w_x^2}\right)^2 - \left(\frac{y - y_0}{w_y^2}\right)^2 - \left(\frac{z - z_0}{w_z^2}\right)^2\right].$$

The initial pulse is launched below the transition region at (x_0, z_0). Its widths along the x- and z-directions are denoted by by w_x and w_z, respectively. In both cases w_y tends to infinity (for better comparison). Parameters of the initial pulse are summarized in Table II.

TABLE II

Parameters of the initial pulse in the 2D and 3D cases.

A_m	$0.5\ c_\mathrm{sc}$
x_0	25 Mm
y_0	—
z_0	2 Mm
w_x	2 Mm
w_z	2 Mm

3. Numerical results

We obtain numerical results with a use of the code ATHENA which was developed by Gardiner and Stone [17]. Athena is based on a single step, second-order accurate Godunov scheme for ideal MHD. This scheme combines the corner transport upwind method for multidimensional integration, and the constrained transport algorithm for preserving the divergence-free constraint on the magnetic field.

To represent a 3D (2D) physical region we use an Eulerian box $50\,\mathrm{Mm} \times 40\,\mathrm{Mm} \times 15\,\mathrm{Mm}$ ($50\,\mathrm{Mm} \times 40\,\mathrm{Mm}$) which is covered by $500 \times 600 \times 30$ (500×600) grid points. We set magnetohydrostatic boundary conditions for all plasma quantities along the x- and z-directions and, if applicable, outflow boundary conditions along the y-direction.

Figures 4 and 5 show mass density and velocity in the loop plane for the 2D and 3D cases, respectively. *A length of arrow is proportional to a magnitude of velocity which is expressed in units of 1 Mm* s^{-1}. The moments of time on both figures are chosen as $t = 100\,\mathrm{s}$ (top panels) and $t = 250\,\mathrm{s}$ (bottom panels).

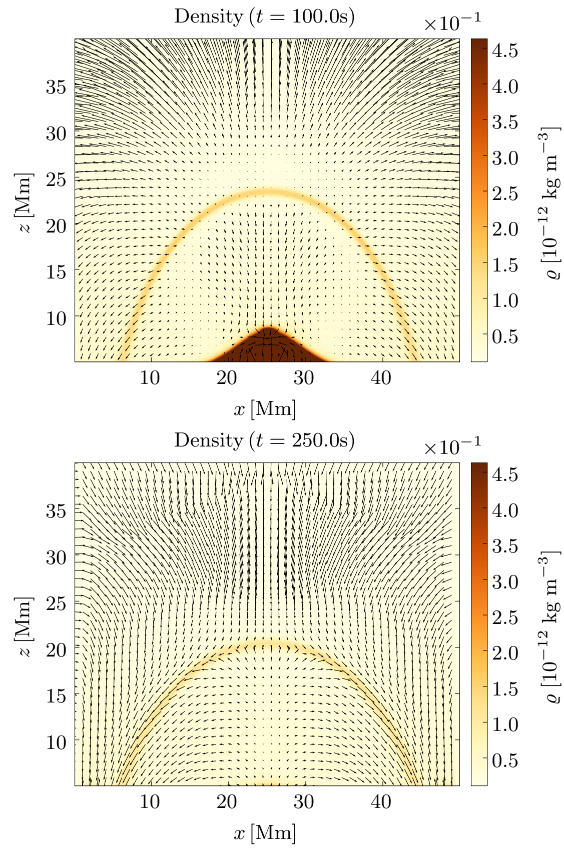

Fig. 4. Mass density and overlying velocity vectors for the 2D loop at $t = 100\,\mathrm{s}$ (top panel) and $t = 250\,\mathrm{s}$ (bottom panel).

Figure 6 illustrates gas pressure (left panels), mass density (right panels) and overlaying velocity vectors for the 3D loop at $t = 100$ s (top panels) and $t = 250$ s (bottom panels). Slices are drawn in the y–z plane that crosses its apex. It is discernible that the movement of the loop is accompanied by the eddies. Such eddies are well known in hydrodynamics.

Figure 7 displays time-signatures of the mass density for the 2D (top panel) and 3D (bottom panel) cases. Numerical data was collected along the line $x = 25\,\mathrm{Mm}$, $y = 7.5\,\mathrm{Mm}$ which passes through the loop apex. Spatial coordinate z and time t are measured in Mm and in seconds, respectively.

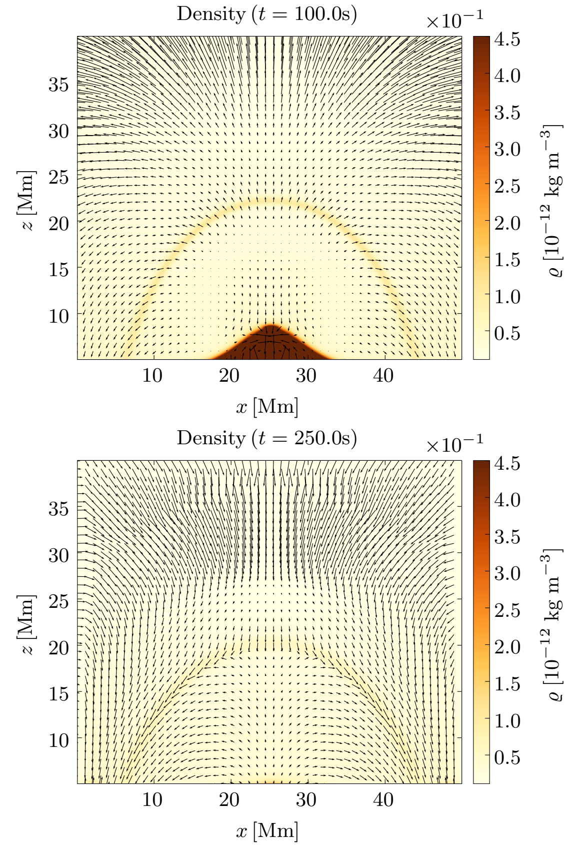

Fig. 5. Mass density and velocity vectors in the $x - z$ plane for the 3D loop for $t = 100$ s (top panel) and $t = 250$ s (bottom panel).

Mass density ϱ is expressed in the unit of $10^{-15}\ \mathrm{kg\,m^{-3}}$. This time-signatures exhibit oscillations which are triggered by the initial pulse. These oscillations decay fast in time.

Figure 8 displays Fourier power spectra of the oscillations of Fig. 7. In the case of 2D and (3D) a main period is 93 s (188 s).

For the straight slab the wave period can be estimated from

$$P_{\mathrm{slab}} \approx \frac{2l}{\bar{c}_{\mathrm{Ac}}} \approx 120\ \mathrm{s}\,, \tag{16}$$

where l is the initial length of the loop and $\bar{c}_{\mathrm{Ac}}$ is the average Alfvén speed within the loop. In case of the loops considered in this paper $c_{\mathrm{Ac}} = 1 \times 10^3 \mathrm{km\ s^{-1}}$ However, although for the curved slab the above formula is too approximate, it can be used for a qualitative estimation of a wave period for the curved slab.

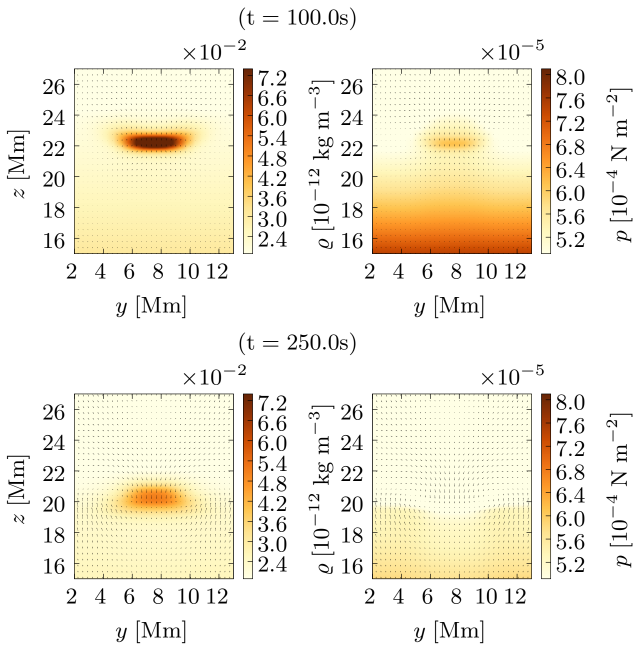

Fig. 6. Slices in the y–z plane (perpendicular to the 3D loop) at $x = 30$ Mm.

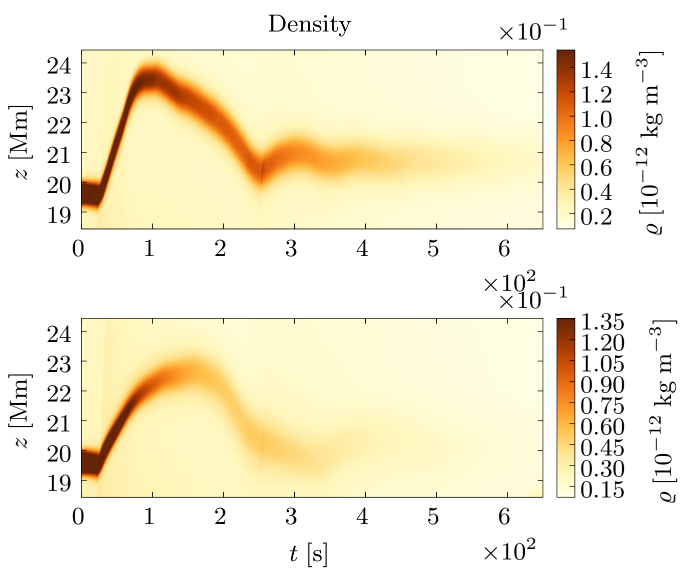

Fig. 7. Time-signatures of a mass density ϱ for the 2D (top panel) and 3D (bottom panel) oscillating coronal loop.

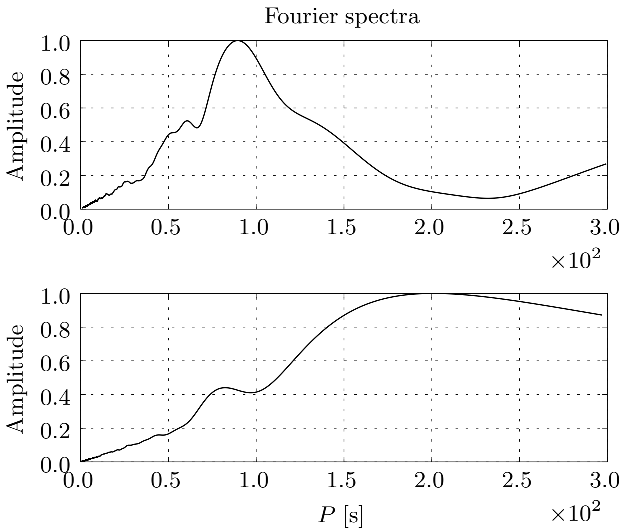

Fig. 8. Fourier spectra of time-signatures of Fig. 7 for the 2D (top panel) and 3D (bottom panel) loops.

4. Summary and discussion

We performed 3D and 2D numerical simulations of vertical oscillations of a solar corona loop. The results are summarized as follows. The initial pulse that is launched below the loop apex triggers a vertical mode of the coronal loop. The amplitude of this mode decays in time. A wave period P of this mode is different in the 3D and 2D cases (Fig. 9).

We found that P scales as $P \sim \varrho_{\rm loop}$, where $\varrho_{\rm loop}$ denotes a loop density. As a result, P attains different values than theoretically expected. A similar scenario was observed in the case of horizontally polarized loop oscillations which were recently showed by Pascoe and De Moortel [12, 13]).

The numerically obtained values of wave periods are smaller than those reported by Ofman and Wang [16] from the Hinode data by about 20%. They specified $P = 1.88$ m $\pm\, 2$ s and $\tau = 9.3$ m $\pm\, 4.3$ m, while the numerical data reveals that $P \simeq 1.5$ m and $\tau \simeq 1$ m. The reason of this departure between the numerical and observational data may lie in a smaller loop we implemented into our model. The observed length was estimated to be 71 Mm with uncertainty about 10–20%, however it may still fit into our simulation where the length was 63 Mm. Also in our case the loop disappears quicker partially because of diffuseness of numerical code we have used and partially because of the way oscillations were excited. After hitting the loop by the initial pulse we observed outflow of plasma from its apex. This on the other case may cause lowered value of damping time τ.

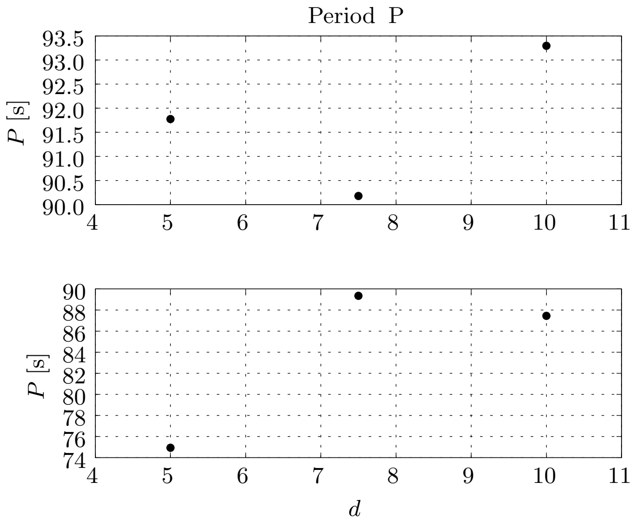

Fig. 9. Wave period P *versus* a loop mass density d for 2D (upper panel) and 3D (lower panel) cases.

P.K. expresses his cordial thanks to Dr. Marcin Gruszecki for a discussion and to Mr. Artur Polak for his assistance in programming. The magnetohydrodynamics code used in this study was developed at the Princeton University by Tom Gardiner, Jim Stone, Peter Teuben and John Hawley with support of the NSF Information Technology Research program. This work was supported by the grant from the Polish State Committee for Scientific Research (KBN), with the Ministry of Science and Higher Education grant for years 2007–2010.

REFERENCES

[1] V.M. Nakariakov, E. Verwichte, *Living Reviews in Solar Physics*, vol. 2, no. 3, 2005.

[2] M.J. Aschwanden, B. de Pontieu, C.J. Schrijver, M. Alan, *Sol. Phys.* **206**, 99 (2002).

[3] C.J. Schrijver, M.J. Aschwanden, A.M. Title, *Sol. Phys.* **206**, 69 (2002).

[4] T.J. Wang, S.K. Solanki, *Astron. Astrophys.* **421**, L33 (2004).

[5] E. Verwichte, C. Foullon, V.M. Nakariakov, *Astron. Astrophys.* **446**, 1139 (2006).

[6] J. Andries, M. Goossens, J.V. Hollweg, I. Arregui, T. Van Doorsselaere, *Astron. Astrophys.* **430**, 1109 (2005).

[7] A.J. Diáz, R. Oliver, J.L. Ballester, *Astrophys. J.* **645**, 766 (2006).

[8] M. Gruszecki, K. Murawski, J. McLaughlin, *Astron. Astrophys.* **489**, 413 (2008).

[9] M. Selwa, S.K. Solanki, K. Murawski, T.J. Wang, U. Shumlak, *Astron. Astrophys.* **454**, 653 (2006).

[10] M. Gruszecki, K. Murawski, *Astron. Astrophys.* **487**, 717 (2008).

[11] L. Ofman, *Astrophys. J.* **694**, 502 (2009).

[12] D.J. Pascoe, I.K. De Moortel, J.A. McLaughlin, *Astron. Astrophys.* **505**, 319 (2009).

[13] de Moortel I. De Moortel, D.J. Pascoe, *Astrophys. J.* **699**, L72 (2009).

[14] L. del Zanna, E. Schaekens, M. Velli, *Astron. Astrophys.* **431**, 1095 (2005).

[15] E.R. Priest, *Solar Magnetohydrodynamics*, D. Reidel, Dordrecht 1982.

[16] L. Ofman, T.J. Wang, *Astron. Astrophys.* **482**, L9 (2008).

[17] T.A. Gardiner, J.M. Stone, *J. Comput. Phys.* **227**, 4123 (2008).